Last author copy

Submitted to Journal of Guidance, Control and Dynamics on April 19th 2014, Accepted on December 23rd 2014

Analytical model for the propagation of small debris objects clouds after fragmentations

Francesca Letizia[1], Camilla Colombo[2], and Hugh G. Lewis[3]
University of Southampton, Southampton, United Kingdom, SO17 1BJ

Current debris evolutionary models usually neglect fragments smaller than 10 cm because of the high computational effort they add to the simulation. However, small debris objects can also be dangerous to operational satellites. This work proposes an analytical approach to describe the evolution of a cloud of small fragments generated by a collision in Low Earth Orbit. The proposed approach considers the cloud globally and derives its evolution analytically, in terms of the change in the spatial density under the effect of atmospheric drag. As a result, the analytical approach allows the representation of small fragments and noticeably reduces the computational time under 10% compared to the numerical propagation of all the fragment trajectories. For altitudes above 800 km the relative error compared to the numerical method is lower than 10%.

---

[1] PhD Candidate, Astronautics Research Group, f.letizia@soton.ac.uk
[2] Lecturer, PhD, currently Marie Curie Research fellow at Politecnico di Milano, Italy, AIAA member, camila.colombo@polimi.it
[3] Senior lecturer, PhD, Astronautics Research Group, h.g.lewis@soton.ac.uk

Nomenclature

A = fragment area [m^2]

a = semi-major axis [km]

a_D = drag acceleration [m/s^2]

c_D = drag coefficient

e = eccentricity

err = relative error

$\mathbf{f}$ = vector field

G = characteristic line of the system

H = scale height for the atmospheric model [km]

h = altitude [km]

i = inclination [rad] or [°]

L_c = fragment characteristic length [m]

M = fragment mass [kg]

M_e = reference mass for collision [kg]

M_p = projectile mass [kg]

$\mu_\square$ = mean of a normal distribution

N_f = fragment number

n = fragment density [-/km]

$n_{f,w}$ = number of fragment in an altitude bin [-]

ν = true anomaly [rad] or [°]

Ω = argument of the ascending node [rad] or [°]

ω = argument of the periapsis [rad] or [°]

R_H = fragmentation distance [km]

r = distance from the Earth [km]

ρ = atmospheric density [kg/m^3]

$\sigma_\square$ = standard deviation of a normal distribution

T_B = time for band formation [s]

t = time [s]

u = longitude of the periapsis [rad] or [°]

v = velocity [m/s]

v_c = collision velocity [km/s]

v_r = radial velocity [km/s]

v_θ = tangential velocity [km/s]

w = width of the altitude bins [km]

Constants

J_2 = second zonal harmonic coefficient of Earth's gravitational potential

μ = gravitational constant [km^3/s^2]

R_E = Earth's radius [km]

I. Introduction

Past space missions left in orbit a large number of non operational objects, whose size varies from large rocket stages to sub-millimeter-size fragments. In Low Earth Orbit (LEO) radars can track objects larger than 10 cm, which are cataloged and monitored, so that they may be avoided with a maneuver in case of risk of collision. Small objects, on the other hand, are not trackable; shields may be adopted on spacecraft to protect them from debris impacts. However, shields are currently adopted only on the International Space Station and, in general, they are effective only for fragments smaller than 1 cm. As a result, a large population of space debris is too big for shields but too small to be tracked and thus poses a risk to operational spacecraft as it may cause for spacecraft anomalies or even more serious damage to satellites [1].

At the moment, already three collisions have been documented between satellites and cataloged fragments plus a collision between two intact satellites, Cosmos 2251 and Iridis 33, that generated more than 2000 new objects [2]. In addition, at least in five occasions a collision between an uncatalogued piece of debris and a satellite was proposed as an explanation of satellite anomalies [3–5]. Therefore, it is important to predict the motion of fragments in orbit and the possible consequence of collisions.

Some research on debris long-term evolution was conducted for the debris population down to 1 cm [6] and 5 cm [7], but most of recent studies neglect objects smaller than 10 cm because their number is so large that the simulation of the debris environment would be extremely expensive in terms of computational time and because the focus has been on the most dangerous impactors [1]. However, this partial representation of space debris environment may result in an underestimation of the collision risk for operational satellites. For this reason, an increasing effort is currently underway to update debris studies by including small objects and to formulate simplified models able to provide quick estimations of space debris evolution.

The prediction of the fragment motion is complex because they have larger area-to-mass ratios than common satellites, so fragments are highly affected by the perturbative forces whose intensity depends on the cross-sectional area, such as atmospheric drag and solar radiation pressure. The analysis of space debris evolution is carried out using numerical methods to consider the perturbation effects on each fragment. Moreover, the shape, the mass and the velocity of a fragment generated by a collision or an explosion can be predicted only with high level of uncertainty, so statistical methods (e.g. Monte Carlo method) are required to obtain reliable results [1]. For these reasons, the simulation of debris population evolution is demanding in term of computational time and only the largest fragments are propagated.

II. Techniques for debris propagation

Some debris models (e.g., SDM [8], DAMAGE [9], DELTA [6]) are able to deal with small fragments grouping them into representative objects, from whose propagation it is possible to re-build the evolution of small objects. For example, an effective technique to reduce the computational time is the method proposed by Rossi et al. [8] where the fragment propagation is simplified in three ways:

- only the most relevant perturbation, drag, is considered to study the fragment motion in LEO,
- the dynamics considered makes use of analytical expressions obtained by King-Hele [10] to describe the secular effect of atmospheric drag,
- only some representative objects are propagated.

The debris population is divided into bins in altitude and object size and only one object per bin is propagated. The result of the propagation is used to estimate how fragments move among the bins; from this, together with the launch frequency and explosion and collision rates for each bin, the evolution of the object number per bin is obtained. In this way, a cloud of more than 800 objects is propagated for 100 years in less than 10 s [11].

Kebschull et al. [12] have further developed this approach, considering also active debris removal, dividing debris objects into eccentricity bins and distinguishing between intact objects and fragments. Moreover, the parameters in the evolution equations were obtained through a fitting process of the full numerical model LUCA; in this way, the output of the simplified model is coherent with the full numerical one, but the simulation time is strongly reduced.

Similarly, Lewis et al. [13] used the data generated by the numerical model DAMAGE to build the simplified model CONCEPT, which is able to study the consequences of a single collision event. Although the current implementation considers only objects larger than 10 cm, this approach can be extended to smaller fragments. The simulation of the fragmentation event is divided into two phases. In the first one, which is valid for all the tested scenarios, the background debris population is built from multiple runs of DAMAGE, whose output is stored in bins of altitude, right ascension and declination: for each bin the distribution of relevant quantities (e.g., spatial density, collision probability, object type, mass, area, orbital parameters) is stored. Secondly, CONCEPT is used to simulate a specific event. It is able to estimate the most likely parameters (i.e., mass and energy) for the fragmentation event. At this point, DAMAGE is used again to generate the debris cloud and to propagate numerically only the new fragments; at each time step the distributions stored in the bins are updated with the contribution from the new cloud, so that it is possible to assess the impact of the simulated event on the global population. As the background population is not actually propagated, but derived from DAMAGE, CONCEPT requires only five minutes to propagate a typical scenario for 200 years.

These two last examples rely on several runs of a full model, whose output is then stored and used by the simplified model. This implies that if part of the full model changes (for example, the breakup model), it should be run again to obtain updated parameters.

Another analytical approach is the one proposed by Hoots and Hansen [14]: in this case, the focus is on the short term evolution of the cloud during the first days after the collision. In this phase the cloud is quite dense and it can increase largely the local collision risk. The evolution of the cloud bounds in the two-body problem is obtained and it defines the most dangerous areas for operational satellites. Perturbations are not considered so this approach is valid only, as said, in the first days of cloud evolution and it is applied only in GEO.

A more radical analytical approach was proposed by Valk et al. [15], who write a Hamiltonian formulation for the dynamics of space debris under the effect of gravity potential (considering J_2 and J_{22}), luni-solar perturbation, and solar radiation pressure. Drag is not considered, as it is not a conservative force, so this model is not applicable for LEO, but it allows a fast evaluation of the debris population in GEO region over several hundreds of years.

Similarly, Izzo proposes a method that describes the debris population globally through the definition of some density functions; the propagation of the population is performed by studying how the density functions in ω and Ω change under the effect of the Earth's oblateness [16] . As also in this case drag is not considered, the method is applicable only in the GEO region.

However, LEO can be considered as the most crucial area for space debris study. First of all, the density of fragments is much higher in LEO than in GEO and in some regions, e.g., synchronous orbits, it is likely to be very close to the critical value for cascading [17], that is the density is so high that the collisions among fragments create more new objects than the ones that are removed by drag. Secondly, the ISS is in LEO and its protection from space debris is essential both for the presence of astronauts and for the delicate experiments, which need to be interrupted in case of collision avoidance maneuver [18]. Finally, the relative velocity is much higher in LEO than in GEO and so collisions tend to be more dangerous [19].

In the literature, only one fully analytical model appears to be applicable in LEO and it was proposed by McInnes [20]: the central idea of this approach is considering the debris population as a fluid with continuous properties. In this way, the analysis of the single objects is abandoned and the fragment density becomes the only parameter of study.

The evolution of the density is obtained through the continuity equation, a traditional approach of fluid dynamics. In particular, if n represents the fragment density, the continuity equation can be written as

$$\frac{\partial n}{\partial t} + \nabla \bullet \mathbf{f} = \dot{n}^{+} - \dot{n}^{-} \tag{1}$$

where $\nabla \bullet \mathbf{f}$ accounts for the *slow*/continuous phenomena (e.g. drag effect) and $\dot{n}^{+} - \dot{n}^{-}$ the *fast*/discontinuous event (e.g. the injection of new fragments due to launches). Once the initial distribution of n is known, the continuity equation is used to obtain its evolution with time, with very low computational effort.

The method is quite general and it has been applied also to describe the evolution of interplanetary dust [21, 22], nano-satellites constellations [23] and high area to mass spacecraft [24] as, in all these cases, continuous and/or discontinuous phenomena has to be described.

Starting from the important results of McInnes [20], the present work aims to move the scope from the global debris population to a single fragmentation event. This is done because for an analytical method is extremely difficult to consider all the aspects (e.g. all the perturbations or the removal of a specific piece of debris) that affect the evolution of the global debris population. From this point of view, the evolutionary debris models previously cited (e.g., SDM [8], DAMAGE [9], DELTA [6]) offer the best results. On the other hand, the analytical propagation based on the continuity equation can be exploited by the evolutionary models to include also small fragments in their analysis. In the analytical method, in fact, the state variable of the problem is the density of fragments and so the computational time is not affected by the considered number of fragments. By also accounting for the contribution of small fragments, the evaluation of the consequences of a single event can be improved and the estimation of the collision risk can be more accurate.

Changing the application from the evolution of the total population to a single event requires some important changes to the method proposed by McInnes [20]. First of all, the method should be able to simulate the production of fragments due to the collision; then, the arbitrary initial distribution used by McInnes [20] should be substituted with the actual distribution of fragments,

which depends on the characteristics of the simulated fragmentation event; only at this point the propagation based on the continuity equation can be applied to obtain an analytical expression for the cloud evolution and a fast evolution of the collision risk for operative spacecraft.

The paper is organized as follows: Section III describes in detail the proposed method, Section IV shows the method results and Section V a comparison with the numerical approach, Section VI discusses the effect of eccentricity on the method accuracy.

III. Analytical approach

The proposed analytical debris model (CiELO, debris Cloud Evolution in Low Earth Orbits) can be represented as in the block diagram in Figure 1, where four main building blocks are presented:

- a break up model that generates the fragment properties (i.e., number, mass, area, speed) given the energy of the collision;
- a numerical propagator to describe the evolution with time of the fragment orbital parameters until the analytical propagation becomes applicable;
- a method to translate the information on the orbital parameters of each single fragment into a continuous density function, useful to compute the collision risk associated to the cloud;
- a fully analytical propagator to express the evolution with time of the cloud spatial density on the long term.

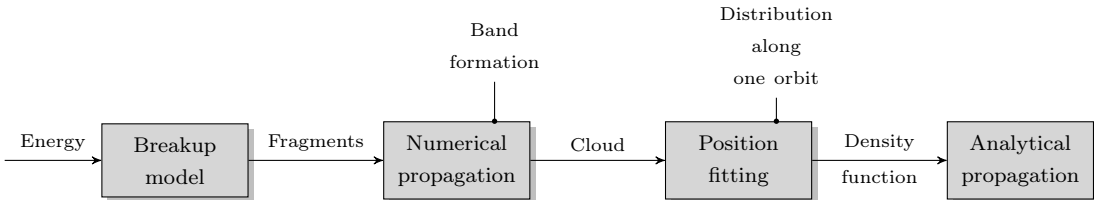

Fig. 1 CiELO building blocks.

This article describes all the method building blocks and evaluates its accuracy and applicability to the description of debris cloud evolution.

A. Breakup model

The model here adopted is the NASA breakup model [25, 26]. It was implemented considering non-catastrophic collisions, which are the ones where the ratio between the kinetic energy and the target mass is lower than 40 J/g. The choice of studying non-catastrophic collisions is also driven by the recent observations that most of the recorded past collisions were non-catastrophic [2]. Only fragments with size in the range from 1 mm to 8 cm are considered, to avoid the discontinuities present in the model and to study how the distributions present in the NASA breakup model influence the fragment dispersion. No mass conservation correction is applied as here not all the cloud is produced and the correction acts mainly on fragments larger than 10 cm[26], not considered here.

The number of fragments N_f larger than a characteristic length L_c produced by a collision is given by

$$N_f(L_c) = 0.1(M_e[\text{kg}])^{0.75}(L_c[\text{m}])^{-1.71}; \tag{2}$$

where M_e is the reference mass of the collision. For M_e, Johnson and Krisko [25] report

$$M_e[\text{kg}] = M_p[\text{kg}](v_c[\text{km/s}]/1[\text{km/s}]) \tag{3}$$

where M_p is the projectile mass and v_c the collision velocity. The expression was then corrected by Krisko [26] as

$$M_e[\text{kg}] = M_p[\text{kg}](v_c[\text{km/s}]/1[\text{km/s}])^2 \tag{4}$$

and this last version is here used [*]. The NASA breakup model provides also the distributions of area-to-mass ratio A/M, which is modeled as lognormal distribution function with mean value $\mu_{A/M}[\text{m}^2/\text{kg}]$ and standard deviation $\sigma_{A/M}[\text{m}^2/\text{kg}]$ depending on the characteristic length L_c. In

[*] Krisko, Paula (2013), personal correspondence of June 10$^{\text{th}}$, Sr. Scientist Specialist, Orbital Debris Modeling Lead, JSC/JETS/Jacobs Tech

particular, for objects smaller than 8 cm, their value is [25]

$$\mu_{A/M} = \begin{cases} -0.3, & \lambda_c \leq -1.75 \\ -0.3 - 1.4(\lambda_c + 1.75), & -1.75 < \lambda_c < -1.25 \\ -1.0, & \lambda_c \geq -1.25 \end{cases} \tag{5}$$

$$\sigma_{A/M} = \begin{cases} 0.2, & \lambda_c \leq -3.5 \\ 0.2 + 0.1333(\lambda_c + 3.5), & \lambda_c > -3.5. \end{cases} \tag{6}$$

with $\lambda_c = \log_{10}(L_c)$. Similarly, the velocity variation distribution is modeled as lognormal distribution function with mean value

$$\mu_v[\mathrm{km/s}] = 0.2 \log(A/M) \tag{7}$$

and $\sigma_v[\mathrm{km/s}] = 0.4$. In this work the ejection velocity direction is randomized and a maximum ejection velocity is introduced, equal to $1.3\, v_c$; this is done because without any limit the method generates a small number of fragments with very high ejection velocity (in the order $60\,\mathrm{km\,s^{-1}}$). This practice is commonly adopted in different implementations of the NASA breakup model [27].

The limits of the NASA breakup model, especially in the sub-centimeter range, are known: it is based on a limited database, so it is not clear how representative the model is [28]. For this reason, some studies are ongoing to improve the model, adding more data points or introducing some physical equations (e.g., the momentum conservation) [28, 29]. However, at the moment no better breakup model is available and the NASA model can be considered as a standard as it is the most used in space debris models [30] (LEGEND, MASTER, DAMAGE). Moreover, the analytical method proposed here does not rely on a specific breakup model: any alternative model, as for example IMPACT [31], can be implemented changing only the first block shown in Figure 1, whereas the other blocks would not require any modification.

B. Numerical propagation

Immediately after the collision, the fragments form a dense cloud concentrated in the location where the breakup occurred (Figure 2a): as each fragment has a slightly different energy, the cloud is stretched along the orbit of the parent spacecraft. In addition, the Earth's oblateness causes a variation of the argument of periapsis ω (Figure 2b) and of the longitude of the ascending node Ω, so that the cloud is finally spread into a band around the Earth (Figure 2c). As a result, ω, Ω and the true anomaly ν are randomized, usually after few months; starting from this point drag can be considered as the dominant perturbation [32]. The analytical method, which represents only the drag effect, can be applied only from this moment, while numerical propagation is required to follow the first phases of the cloud evolution.

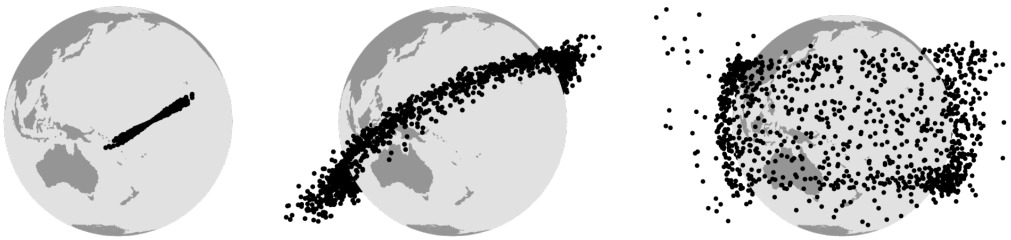

(a) Ellipsoid (b) Toroid (c) Band

Fig. 2 Phases of debris cloud evolution as classified by Jehn [32].

The fragment orbital parameters are propagated numerically using Gauss' equations [33]: for the Earth's oblateness, only J_2 is considered because, as said before, the transition to the band occurs in a few months. The drag effect is computed through King-Hele's expressions [10] for eccentricity e lower than 0.2; no atmospheric rotation is considered; the maximum altitude below which drag is considered is 1000 km and the propagation is stopped if the fragment perigee altitude is below 50 km as re-entry occurs. For the atmospheric density ρ, an exponential model is used

$$\rho = \rho_{\text{ref}} \exp\Big(- \frac{h - h_{\text{ref}}}{H} \Big) \tag{8}$$

where h is the altitude, h_{ref} is the reference altitude where the reference density ρ_{ref} and the scale height H are defined. The reference values $h_{\text{ref}}, \rho_{\text{ref}}, H$ and are taken from Vallado [33] and h_{ref} is set as the altitude where the collision occurs and its value is kept constant for the whole simulation.

These settings are used also for the full numerical simulation of the cloud evolution used to validate the analytical approach. The approximation of constant $h_{\text{ref}}, \rho_{\text{ref}}, H$ will be relaxed; here it is kept for simplicity as the aim of the present work is to validate the proposed analytical model against the numerical simulations.

The numerical propagation is terminated when the band is formed, so when the condition in Figure 2c is reached: this can be verified numerically comparing the distribution of the angles (ν, ω, Ω) with a uniform distribution between $-\pi$ and π. The true anomaly ν is not considered as its dispersion (transition from Figure 2a to Figure 2b) is much faster. The distributions of ω, Ω are instead evaluated through the Kolmogorov-Smirnov test, which measures the maximum distance between the *empirical* cumulative distribution function of the tested data (in this case the fragment angles coming from the simulations) and a reference cumulative distribution function (in this case the one of the uniform distribution) [34]. When the hypothesis of uniform distribution is valid for both the angles, the band is considered formed. However, this would require propagating all the fragments instant by instant, whereas here the propagation is done fragment by fragment, exploiting the possibility of parallelizing the code and reducing remarkably the computational time. For this reason, the proposed approach requires an *a priori* criterion to stop the numerical propagation, based only on the knowledge of the initial orbit. Some estimations [35–37] are available in literature for this purpose and they rely on the hypothesis that apsidal and nodal dispersion is complete when the faster fragment, in terms of apsidal/nodal rate, encounters the slowest one. In particular, Ashenberg [37] gives an analytical expression to estimate the time for band formation T_b as a function of the orbital parameters of the initial orbit. T_b is defined as the maximum between the time of the dispersion of the longitude of the ascending node Ω (T_Ω) and the one of the argument of periapsis ω (T_ω). They are expressed as

$$
\begin{aligned}
T_b &= \max(T_\Omega, T_\omega) \\
T_\Omega &= \frac{\pi}{3J_2 \frac{R_E^2}{a^3}(7\cos i \cos\beta_\Omega + \sin i \cos u \sin\beta_\Omega)\Delta v} \\
T_\omega &= \frac{\pi}{3J_2 \frac{R_E^2}{a^3}(7(2 - \frac{5}{2}\sin^2 i)\cos\beta_\omega + \frac{5}{2}\sin 2i \cos u \sin\beta_\omega)\Delta v}
\end{aligned}
\tag{9}
$$

where

$$\begin{aligned} \tan\beta_\Omega &= \frac{1}{7}\tan i\cos u \\ \tan\beta_\omega &= \frac{5\sin 2i\cos u}{14(2-\frac{5}{2}\sin^2 i)} \end{aligned} \tag{10}$$

and R_E is the Earth's radius; a, i, u are respectively the semi-major axis, the inclination and the longitude of the periapsis of the orbit where the fragmentation occurs; Δv is the impulsive variation in velocity due to the breakup. Ashenberg [37] assumes that the breakup can be treated as an isotropic explosion with the same Δv for all fragments. Here, the breakup model computes different values of velocity variation for each fragment and so an average value is used in Equation 9. The dependence of T_b on the altitude and on the inclination of the initial orbit is shown in Figure 3, which is obtain with $\Delta v = 0.46\,\mathrm{km/s}$.

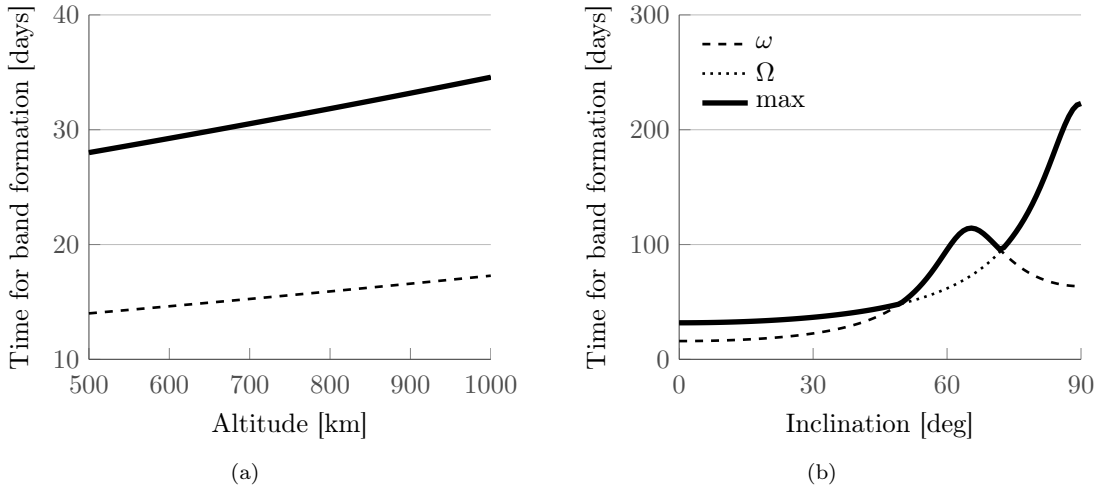

Fig. 3 Days required to form the band, according to Ashenberg [37], as a function (a) of the fragmentation altitude and (b) of the inclination of the parent orbit.

The accuracy of these analytical expressions can be evaluated comparing them with the numerical estimation T_{KS} obtained with the Kolmogorov-Smirnov test (Figure 4); in particular, the band is considered formed at time from which the Kolmogorov-Smirnov test is true for at least 90% of the following instants. The analytical expressions underestimate the time to form the band because, as explained by Jehn [32], when the fastest particle meets the slowest one, the fragments are not yet distributed uniformly in ω and Ω. To define a stop criterion for the numerical propagation of the

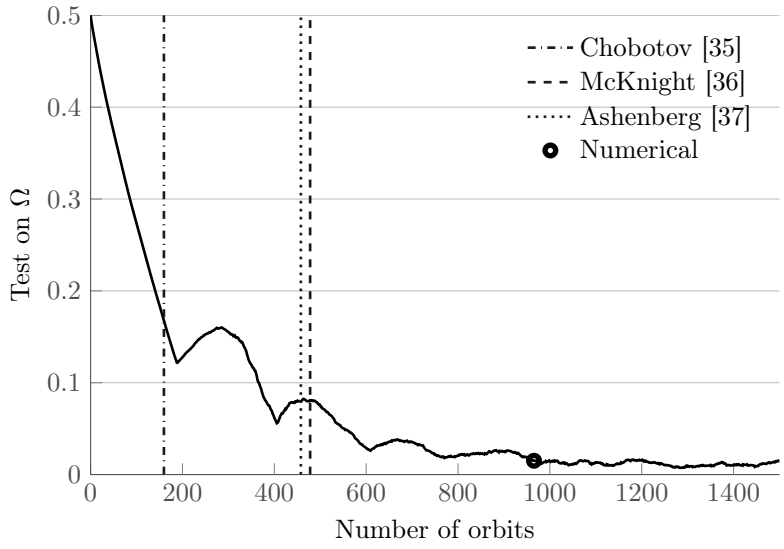

Fig. 4 Kolmogorov-Smirnov distance for the ascending node Ω with number of orbits N.

cloud up to band formation that does not involve a continuous check on the results, several scenarios were run for different altitudes and inclinations to estimate a safety factor to apply to Ashenberg's prediction. From Figure 5 three was chosen as a reasonable value for n_{KS}, so the band formation time for the CiELO model is set to $T_B = 3T_b$.

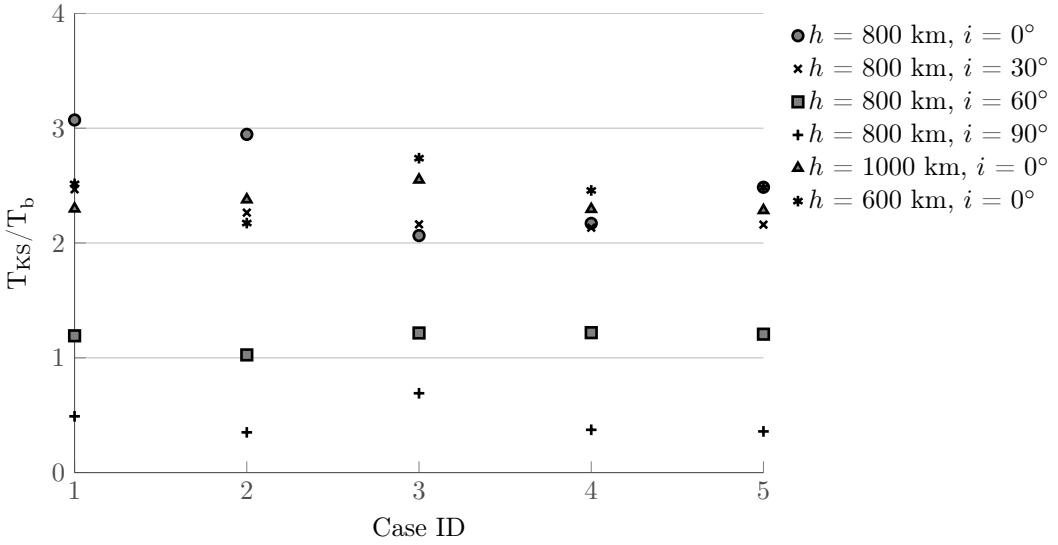

Fig. 5 Ratio between the numerical estimation of the time for band formation T_{KS} and the analytical one T_b as in Equation 9. Five runs of the NASA breakup model were executed for each scenario.

It is anyway interesting to verify what happens if the initial condition is built using different values of the safety factor n_{SF}. The cloud density profile was compared at four time intervals with

different values of n_{SF}. Figure 6 shows the relative error compared to the results for $n_{SF} = 4$: the error is measured on the number of fragment each altitude bin (large 25 km) that form the domain. Note that, since the relative error is computed bin-wise, the peaks in the relative error for some altitudes are not due to large differences between the curves, but to errors in the location of the peak in the density profile. This was easily verified by comparing the overall shape of the density profiles, evaluating their integral. The relative error on the integral between the cases with $n_{SF} < 4$ and the reference case with $n_{SF} = 4$ is always lower than 3%, so the method appears quite robust to the choice of the initial condition.

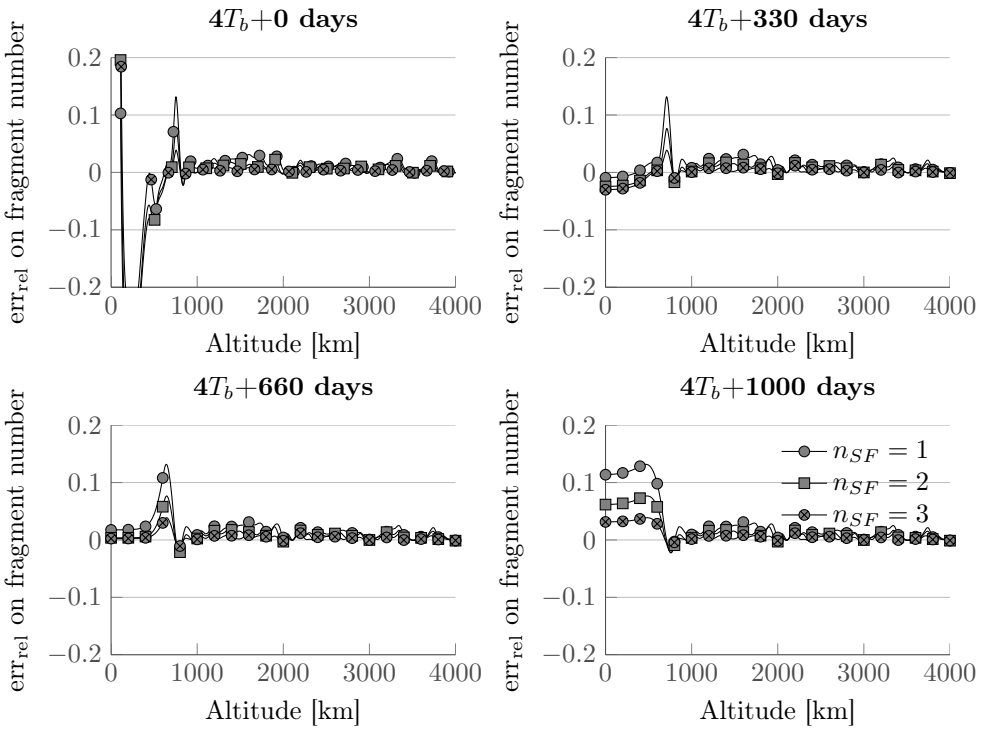

Fig. 6 Relative error on cloud density profile at four time intervals with four different values of n_{SF} for a fragmentation at 800 km. The reference profile is the one obtained with $n_{SF} = 4$.

C. Position fitting

Once the band is formed, the information on the fragment positions is translated into a continuous density function that will be the initial condition for the analytical method. In the previous version of the proposed model [38], the density function was built from the distribution of fragments in distance from the Earth r or semi-major axis a, whereas here it is built on the probability of find-

ing fragments at a certain altitude. In fact, if only one coordinate is considered, this representation can be easily used to compute the impact of the cloud on the collision risk for operational satellites.

The probability density for a cloud is built starting from the expression by McInnes and Colombo [39] describing the number density of objects along one orbit with eccentricity e_i and semi-major axis a_i,

$$n_{\nu,i}(\nu) = \frac{(1+e_i)^2}{(1+e_i\cos\nu)^2}, \tag{11}$$

where the density expression is selected such that $n_{\nu,i}(\nu = 0) = 1$. Equation 11 expresses the condition that, as an object is slower close to the apogee, it spends more time in that region of space and so there is higher probability of interception. Equation 11 can be easily expressed in terms of the distance from the Earth r as

$$n_i(r) = \begin{cases} \frac{3}{2}\frac{r^2}{a_i^3(3e_i+e_i^3)}, & \text{if } a(1-e) \leq r \leq a(1+e) \\ 0, & \text{otherwise} \end{cases} \tag{12}$$

where the density is rescaled so that the integral of the expression in Equation 12 between the perigee and the apogee radius is equal to 1. In this way, it is possible to sum the contribution from each fragment to obtain the probability density for the whole cloud (Figure 7a) as

$$n(r) = \sum_i^N n_i(r) \tag{13}$$

where N is the total number of fragments.

Besides the connection with collision risk computation, this approach presents an additional advantage: the initial condition built in terms of probability density is less dependent on the single run of the break up model compared to the one built on the semi-major axis or on the distance. The breakup model contains in itself some random values (e.g., to define the fragment distribution in terms of ejection velocity) and so more runs are required to generate data with statistical meaning. Figure 7 presents the comparison among three possible initial conditions; three different runs of

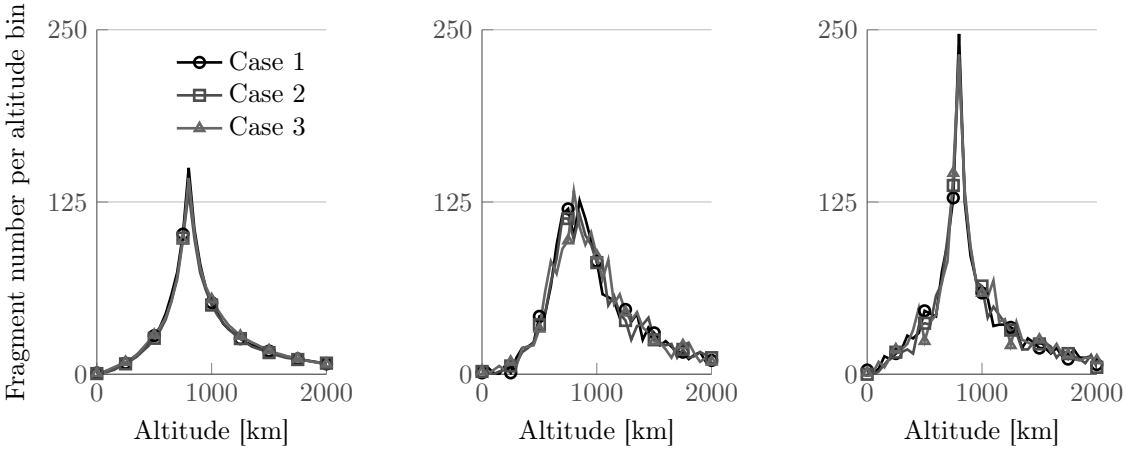

(a) Probability (b) Semi-major axis (c) Distance

Fig. 7 Comparison among three different distributions that may be used to describe the initial condition: (a) refers to the probability density as defined in Equation 13, (b) to the semi-major axis distribution (as in [38]), (c) to distance distribution (as in [38]). Each marker refers to a different run of the break-up model.

the break-up model are presented, each one plotted with a different marker. It is possible to see that, in contrast to the simple distribution in r (Figure 7c), the probability density (Figure 7a) has only a limited variation with the specific analyzed run; moreover, the distribution in r tends to the probability density if many cases are run and averaged.

D. Analytical propagation

Once the initial fragment density of the band is defined, the continuity equation is used to derive analytically the density evolution with time under the drag effect, following the approach developed by McInnes [23] and here briefly summarized for clarity.

Neglecting discontinuous events (sources, for example launches, and sinks, for example active debris removal), the continuity equation can be written as

$$\frac{\partial n}{\partial t} + \nabla \bullet \mathbf{f} = 0; \tag{14}$$

where n is the fragment density and the term $\mathbf{f}$ is the vector field that causes the fragment position to vary with time t.

The distance r is the only considered coordinate, so a spherical symmetry is assumed; as stated before, this assumption and modeling only drag effect imply that the analytical propagation becomes

applicable after the cloud has formed a continuous band around the Earth. The vector field has then only one component in the radial direction

$$f_r = v_r n(r,t). \tag{15}$$

The drift velocity in the radial direction v_r is obtained from the expression of drag acceleration

$$a_D = \frac{1}{2}\frac{c_D A}{M}\rho(r)v^2 \tag{16}$$

where c_D is the drag coefficient of the fragment, which is assumed to be constant and equal to 2.2 [33]; A is the fragment cross-sectional area; M is the fragment mass; v is the fragment velocity and $\rho(r)$ is the atmosphere density, which depends on the distance from the Earth as in Equation 8. The effect of drag is to reduce the orbit energy $\mathcal{E}$ with a rate equal to

$$\frac{d\mathcal{E}}{dt} = -v_\theta a_D \tag{17}$$

where v_θ is the tangential velocity that, with the hypothesis of quasi-circular orbits, can be considered equal to $\sqrt{\mu/r}$. Always with the hypothesis of quasi-circular orbits, the energy variation can also be written as

$$\frac{d\mathcal{E}}{dt} = \frac{d}{dt}\Big(-\frac{\mu}{2r}\Big) = \frac{\mu}{2r^2}v_r. \tag{18}$$

Combining Equations 17 and 18, the radial velocity can be written as

$$v_r = -2r^2\frac{v_\theta a_D}{\mu}; \tag{19}$$

substituting v_θ and a_D with their expressions and putting $v^2 = v_\theta^2 + v_r^2 \approx v_\theta^2$, the following expression for the radial velocity is obtained

$$v_r = -\sqrt{\mu r}\frac{c_D A}{M}\rho(r). \tag{20}$$

Similarly to McInnes [23], the parameter ε is introduced,

$$\varepsilon = \sqrt{\mu}\frac{c_D A}{M}\rho_{\text{ref}}, \tag{21}$$

which collects all the terms that do not depend on r. Observe that here the definition of ε is slightly different from the original one in McInnes [23] because, to increase the numerical accuracy, it is convenient to compute the exponential term always as $\exp\Big(-\frac{h-h_{\text{ref}}}{H}\Big)$ and not as two separate terms. Putting $R_H = R_E + h_{\text{ref}}$, the final expression for v_r is obtained

$$v_r = -\varepsilon\sqrt{r}\exp\Big(-\frac{r-R_H}{H}\Big). \tag{22}$$

This expression of v_r allows writing the term $\nabla \bullet \mathbf{f}$ in the continuity equation (Equation 14) that becomes

$$\frac{\partial n(r,t)}{\partial t} + \frac{1}{r^2}\frac{\partial}{\partial r}\Big(r^2 v_r n(r,t)\Big) = 0. \tag{23}$$

Performing the derivation and collecting the terms with respect to n, Equation 23 can be rewritten as

$$\frac{\partial n(r,t)}{\partial t} + v_r\frac{\partial n(r,t)}{\partial r} + \Big[\frac{2}{r}v_r + v_r'\Big]n(r,t) = 0, \tag{24}$$

where $()'$ indicates the derivation with respect to r. Equation 24 is a first order linear partial differential equation that can be solved with the method of characteristics, whose expression in this case is

$$G(r,t) = \exp\Big(\frac{r-R_H}{H}\Big) + \varepsilon\frac{\sqrt{R_H}}{H}t, \tag{25}$$

obtained with the approximation

$$\sqrt{r} \approx \sqrt{R_H}. \tag{26}$$

Applying this procedure, McInnes [23] found an explicit expression for the density evolution,

$$n(r,t) = \frac{\Psi\{\exp\left[-\frac{r-R_H}{H}\right] + (\varepsilon\sqrt{R_H}/H)t\}}{-\varepsilon r^{5/2}\exp\left[-\frac{r-R_H}{H}\right]} \tag{27}$$

where the function Ψ is obtained from the initial condition $n(r, t = 0)$ and the characteristics z at $t = 0$

$$z = G(r,0) = \exp\Big(\frac{r-R_H}{H}\Big), \tag{28}$$

so that

$$\Psi(z) = \frac{n(r(z),0)}{r(z)^2 v_r(z)}. \tag{29}$$

Equation 27 provides a fully analytical expression to compute the effect of drag on the cloud and the analytical propagation always acts on the cloud globally, not on the single fragments. Therefore, in this case, the model is *analytical* in the sense that, once the initial density is known, the cloud density at any time is immediately known, without any numerical integration of the fragment trajectories, differently from previous models [8, 12, 13].

Moreover, Equation 29 shows that no particular operation is needed on the function $n(r, 0)$, providing large flexibility on the functions that can be used to describe the initial condition. This means that the initial condition can be built easily starting from different kind of fragmentation phenomena. It is important to observe that the shape of the initial condition is used only as a starting point for the analytical method, which is able to modify the function shape to follow the cloud evolution. This point can be demonstrated considering a case where the initial condition is defined by a normal distribution

$$n(r,0) = n_m \exp\left[-\lambda(r-R_H)^2\right] \tag{30}$$

where n_m is a scale factor and R_H the fragmentation distance as before. The expression for n in

Equation 27 can be rewritten as

$$n(r,t) = n_m \exp\Big\{ -\lambda\Big[H\log\Big(\exp\Big[\frac{r-R_H}{H}\Big] + \varepsilon\frac{\sqrt{R_H}}{H}t\Big)\Big]^2\Big\}\cdot \\ \cdot \Big[H\log\Big(\exp\Big[\frac{r-R_H}{H}\Big] + \varepsilon\frac{\sqrt{R_H}}{H}t\Big) + R_H\Big]^{5/2} \frac{1}{\exp\Big[\frac{r-R_H}{H}\Big] + \varepsilon\frac{\sqrt{R_H}}{H}t} \frac{1}{r^{5/2}\exp\Big[-\frac{r-R_H}{H}\Big]}. \tag{31}$$

Introducing

$$\tilde{z} = H\log\Big(\exp\Big[\frac{r-R_H}{H}\Big] + \varepsilon\frac{\sqrt{R_H}}{H}t\Big) + R_H \tag{32}$$

the Equation 31 becomes

$$n(\tilde{z}) = n_m \exp\left[-\lambda(\tilde{z}-R_H)^2\right]\frac{\tilde{z}^{5/2}}{\exp\left[z-\tilde{R}_H/H\right]}\cdot\Big(\exp\Big[\frac{\tilde{z}-R_H}{H}\Big] + \varepsilon\frac{\sqrt{R_H}}{H}t\Big)\cdot \\ \cdot\Big[H\log\Big(\exp\Big[\frac{\tilde{z}-R_H}{H}\Big] - \varepsilon\frac{\sqrt{R_H}}{H}t\Big) + R_H\Big]^{5/2} \tag{33}$$

and so the shape of the initial condition ($n_m \exp\left[-\lambda(\tilde{z}-R_H)^2\right]$) is modified by a factor that depends on the dynamics of the problem.

It is also important to notice that, the parameter ε, defined in Equation 21, is not constant for the whole cloud as the fragments have different area-to-mass ratios, A/M. To improve the accuracy of the model, N bins in area-to-mass ratio are here defined. For each bin, an average ε_i is assumed and the corresponding density n_i is obtained according to Equation 27; all the partial densities n_i are summed to obtain the global cloud density n.

$$n(r,t) = \sum_i n_i = \sum_i \frac{\Psi\{\exp\left[-\frac{r-R_H}{H}\right] + (\varepsilon_i\sqrt{R_H}/H)t\}}{-\varepsilon_i r^{5/2}\exp\left[-\frac{r-R_H}{H}\right]} \tag{34}$$

Different definitions of the bins are possible: in particular, two options were tested and compared:

- same fragment number: the bins in A/M are defined so that each one contains the same number of fragments at the band formation,

- logarithmically spaced: the edges of the bins are defined as logarithmically spaced intervals having as maximum/minimum valued the maximum/minimum of the fragment population at the band formation.

Figure 8 shows the method accuracy and the computational time as a function of the number of bins, defined with the two described approaches. The accuracy is measured through the relative error between the integral of the density profile obtained with the analytical method and the integral of the profile obtained with the numerical propagation (error on total) and through the relative error on the density peak height as explained more in detail in Section V B. The Figure shows that the first approach (same number of fragment in each bin) has a lower error than the logarithmically spaced bins and so it is used in the following. Figure 8 allows also choosing the optimal number of bins and it was set equal to 10: for this value there is a convenient reduction of the error compared to using a single value of ε for the whole cloud and the computational time is only slightly affected.

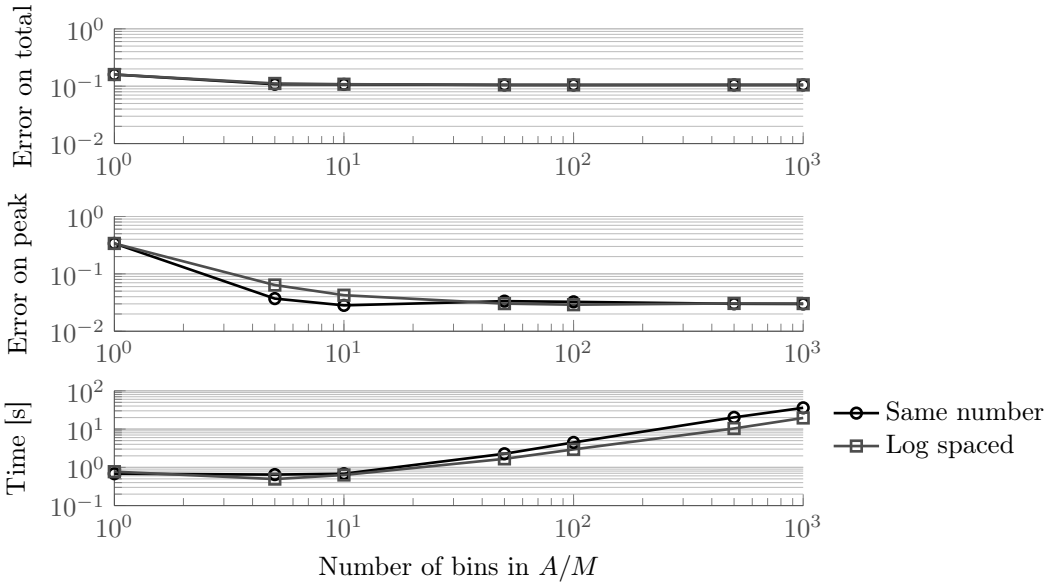

Fig. 8 Relative error on density peak, relative error on the total number of fragments and computational time as a function of the number of bins in A/M.

IV. Results for a fragmentation at 800 km

The results in this section refer to a fragmentation generated by the non-catastrophic collision between a spacecraft and a projectile of 100 g with a collision velocity of 1 km s^{-1}. The parent orbit of the spacecraft is planar and circular, with altitude equal to 800 km. At this altitude, according

to the used atmosphere model, the scale heigh is $H = 124.64\,\mathrm{km}$ and the atmosphere density is $\rho_{\mathrm{ref}} = 1.170 \times 10^{-14}\,\mathrm{kg/m^3}$. The collision generates 2397 fragments, whose area-to-mass ratios range from 0.0298 to $15.4\,\mathrm{m^2\,kg^{-1}}$ in the specific run of the breakup model considered. In fact, all the following results refer to this single run of the NASA breakup model, which is the only stochastic block, as the study aims to compare and validate the analytical propagation against the numerical propagation.

The results are here expressed in terms of the number of fragments ($n_{f,w}$) in a spherical shell of radius r and width w, here set equal to 25 km; it is equivalent to count represent the fragment distribution in altitude with histograms with width w. This output can be translated into the average fragment density d with the following expression

$$d = \frac{n_{f,w}}{V} \qquad V = 4\pi w\Big(\frac{w^2}{12} + r^2\Big). \tag{35}$$

The representation in terms of density is independent on the bin width, but here the representation with the number of fragments is preferred because it provides an easier physical interpretation.

The band is formed after almost 95 days and then the analytical propagation is applied. Figure 9 shows the cloud density, obtained with the analytical method, from the band formation to 1000 days later. At the band formation, Figure 9 indicates a distinct peak (the bright white area) in the cloud density at the altitude of the breakup. After 1000 days, drag has reduced the density peak and also the number of fragments at low altitudes as the area below the fragmentation altitude becomes darker and darker during the cloud evolution; the density at high altitude is, instead, almost unchanged. Figure 9allows also estimating how the altitude range affected by the fragmentation is reduced with time.

More in detail, the evolution of the density profile in time is shown in Figure 10, where the density profiles for all the values of the area-to-mass ratio are shown. It is possible to observe how for low values of A/M there is a clear peak in the density profile also after 1000 days, whereas for high A/M values the peak is less distinct and it is quickly eroded with time.

The number of fragments at the band formation is equal to 1740, which means that 27% of

the fragments generated by the collision decay before the band formation. The analytical method predicts that after 1000 days, 1420 are still in orbit, against the result of 1357 obtained with the numerical integration: the relative error in the estimation of the fragment number is around 10%, so the analytical method can be considered a good approximation. During the 1000 days, the altitude of the density peak is reduced by 34% (Figure 11a); the peak location is basically unchanged (Figure 11b) for the cloud globally, whereas it undergoes a large variation for fragments with high area to mass ratio A/M. This is due to the fact, for the particular choice of the bin definition, the curves referring to high A/M values are more flat and the altitude corresponding to the peak (that is the point with the highest density) changes discontinuously (Figure 10).

Also the shape of the density function is affected by drag, which acts differently at low and high altitude. For this reason, the fragment density is reduced in 1000 days by 33% at an altitude smaller or equal to the parent altitude 800 km and only by 10% for higher altitudes. As the peak is reduced with time, the band of altitudes that contains 68.27%[†] of the population increases its amplitude with time (Figure 12).

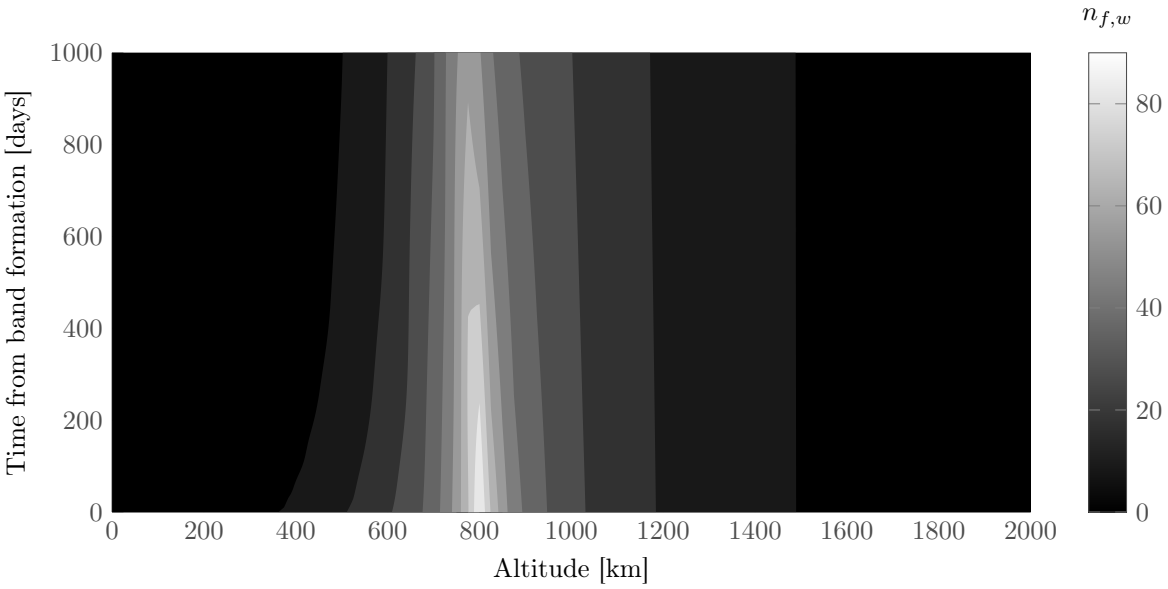

Fig. 9 Visualization of cloud density evolution for a fragmentation at 800 km.

[†] The specific value of the percentage is borrowed from the definition of normal distribution, where 68.27% of the values lie within one standard deviation from the mean.

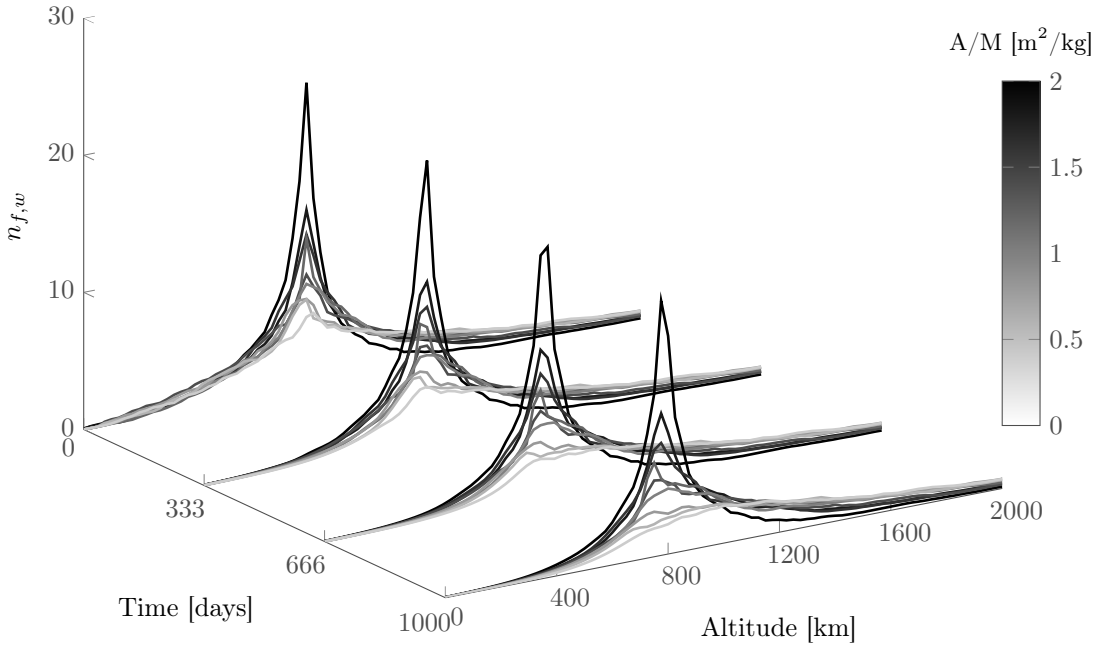

Fig. 10 Evolution of the cloud density as a function of time after the band formation, for a fragmentation at 800 km.

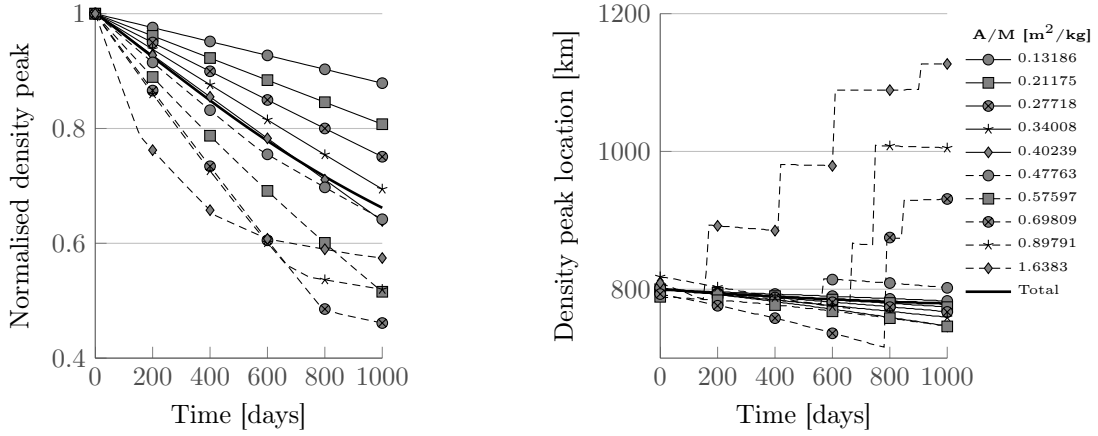

(a) Normalised peak height

(b) Peak location

Fig. 11 Evolution of the density peak height and location for a fragmentation at 800 km. The value of the peak height is normalized with the value at band formation. The black lines refers to the value for the cloud globally.

V. Comparison with numerical propagation

Figure 13 shows the comparison between the numerical (in black) and the analytical (in gray) propagation of the cloud probability density. Globally, the analytical method is able to follow the cloud evolution very well, catching both the reduction of the fragment number and the different effect of drag on low and high altitude.

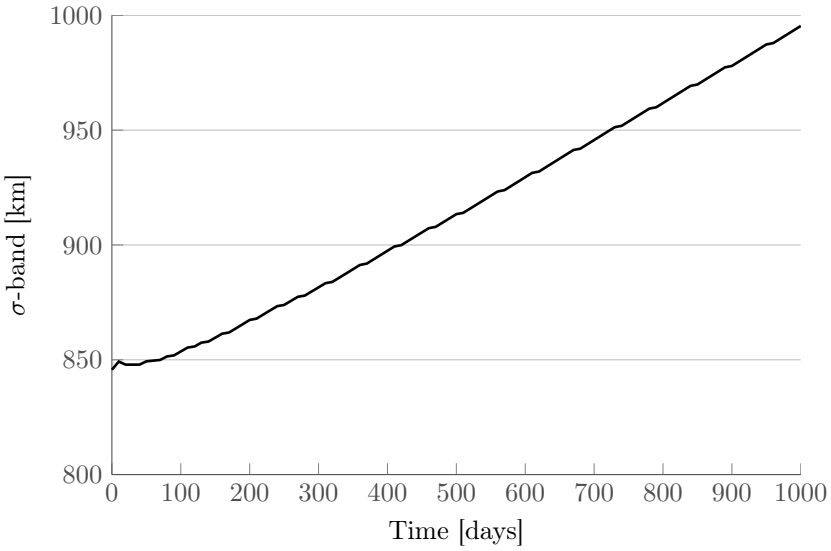

Fig. 12 Evolution with time of the amplitude of the altitude band that contains 68.27% of the population for a fragmentation at 800 km.

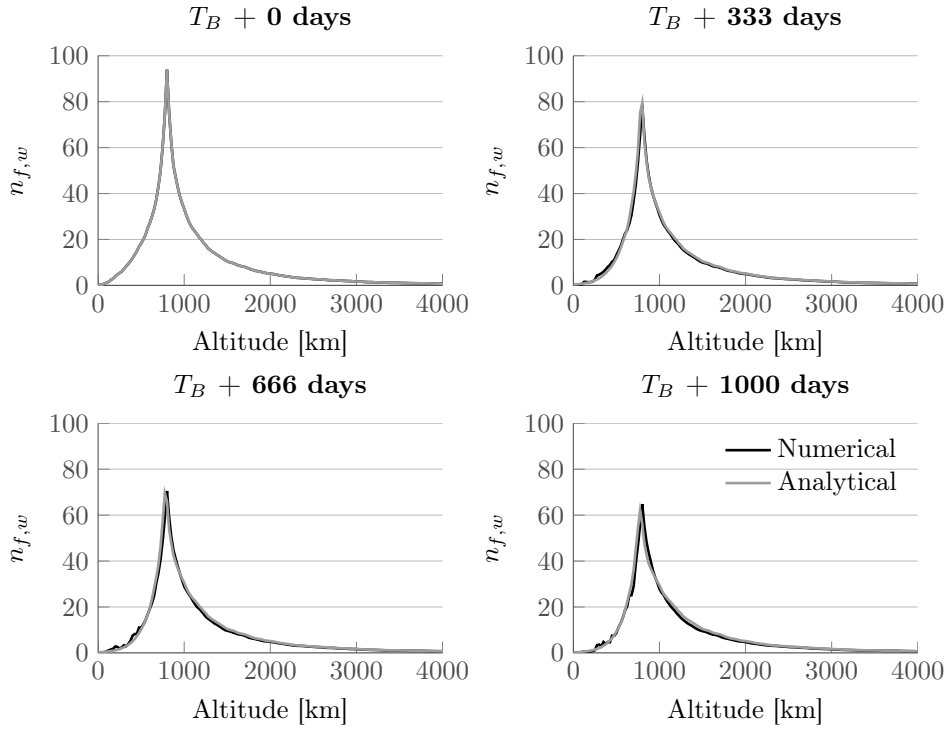

Fig. 13 Evolution of the cloud density as a function of time after the band formation, for a fragmentation at 800 km.

A. Computational time

It is interesting to compare the numerical and the analytical propagation in terms of computational time, as shown in Figure 14: the intervals reported in the diagram refer to the case shown in Figure 13 and Section IV, so the simulation of a cloud of initially 2397 fragments up to 1000 days

after the band formation.

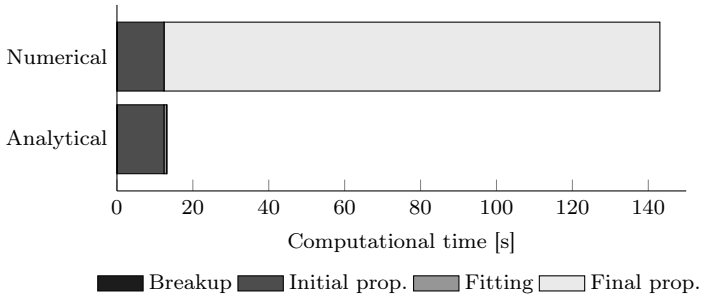

Fig. 14 Computational time for a PC with 8 CPUs at 3.40 GHz.

The measured computational times refer to a PC with 8 CPUs at 3.40 GHz and the code for the numerical propagation is parallelized and written in Matlab. In both cases, the breakup model requires less than 0.1 s to generate the cloud. For the analytical method, the main contribution is given by the initial propagation until the band formation (12.3 s), while the time for the final (analytical) propagation is negligible (0.086 s) and only 0.7 s are required to build the initial condition. On the other hand, the full numerical propagation takes 130 s to simulate 1000 days, as the simulation time for the numerical propagation depends on the number of fragments and the number of days. For this reason, the analytical approach is an efficient tool to simulate different collision scenarios as it will be shown in a future work.

B. Accuracy of the method

Two indicators are used to estimate the method accuracy:

- err_{peak}, which measures the relative error on the peak height, comparing the maximum density value for the analytical and numerical propagation,
- err_{tot}, which measures the relative error on the total number of fragments obtained by integrating the density curve.

The method is considered applicable when both the errors are lower than 20% for the global cloud.

Table 1 summarizes the error values for all the A/M bins and for the cloud globally for a fragmentation at 800 km. It is possible to observe that the analytical model performs quite well in all the bins, even if its accuracy decreases for high A/M bins. This is due to the fact that high A/M

bins correspond to a high mean eccentricity, so the hypothesis of circular orbits, required to write v_r as in Equation 22, introduces a certain level of error. The issues associated with this hypothesis are discussed in the following section, but it is interesting to observe here that the dependency of mean eccentricity on the area-to-mass ratio is a product of how the velocity distribution is written in the NASA break up model [25].

Table 1 Relative error on the density peak and on the density integral after 1000 days for all the values of area-to-mass ratio and for the cloud globally for a fragmentation at 800 km**.**

A/M [m^2/kg]	0.13	0.21	0.28	0.34	0.40	0.48	0.58	0.70	0.90	1.64	Total
$\mathrm{err}_{\mathrm{peak}}$	0.19	0.10	0.10	0.15	0.19	0.14	0.17	0.28	0.21	0.25	0.04
$\mathrm{err}_{\mathrm{tot}}$	0.10	0.10	0.13	0.15	0.15	0.13	0.16	0.19	0.18	0.20	0.10

An analysis of the error for different conditions of fragmentation is shown in the following sections.

C. Range of applicability

The method applicability was tested varying the initial orbit of the impacted spacecraft, both in inclination and in altitude. To highlight the effect of these parameters, the results refer always to same run of the NASA breakup model.

Figure 15 shows the value of error after 1000 days from the band formation for inclination ranging from 0 to 90 degrees: the value is always around 0.10, so the method follows correctly the cloud evolution for all the inclination values. The variation in the errors is related to the fact that the ejection velocity direction is random and it was not kept constant for the different simulations.

Figure 16 shows the value of the errors after 1000 days, but for different orbit altitudes: the altitude has a large effect on the method accuracy and, in general, the method seems to be applicable for altitudes higher than 800 km. This is the region where remote sensing missions are operating from sun-synchronous orbits.

Figure 17 shows a comparison of the density profile after 1000 days for six different altitudes: at low altitudes ($<$ 700 km) the analytical method largely underestimates drag effect, where the analytical method is expected to overestimate the collision probability. It is interesting to observe that the error is large in relative terms, but small in absolute one as, for example, in the case at

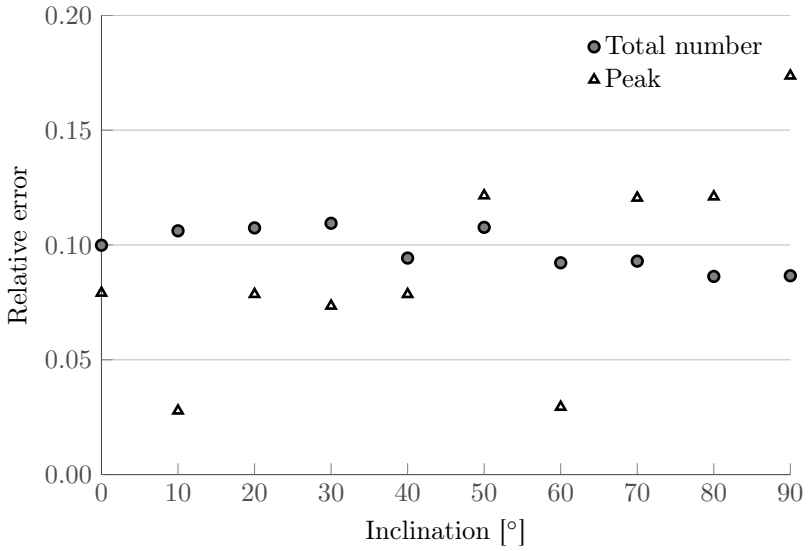

Fig. 15 Accuracy of the method, measured by the relative error after 1000 days from the band formation, as a function of the inclination of the orbit where the fragmentation occurs (with fixed altitude equal to 800 km).

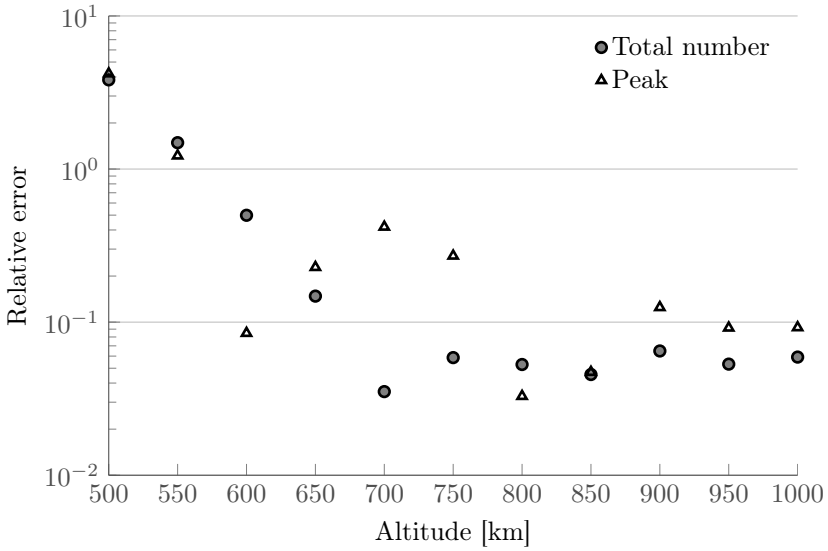

Fig. 16 Accuracy of the method, measured by the relative error after 1000 days from the band formation, as a function of the fragmentation altitude.

500 km only 123 fragments are left after 1000 days and the error on the peak equals five fragments. Drag effect is, instead, overestimated in the case at 700 km. For all the cases at high altitudes ($\geq$ 800 km) there is a very good agreement between the numerical and the analytical propagation.

As anticipated at the beginning of the section, the threshold value for the errors was fixed at 20% and this limit can be used to estimate the maximum simulation time length at different altitudes. Figure 18 shows the result of this analysis: for a fragmentation at 500 km the errors are

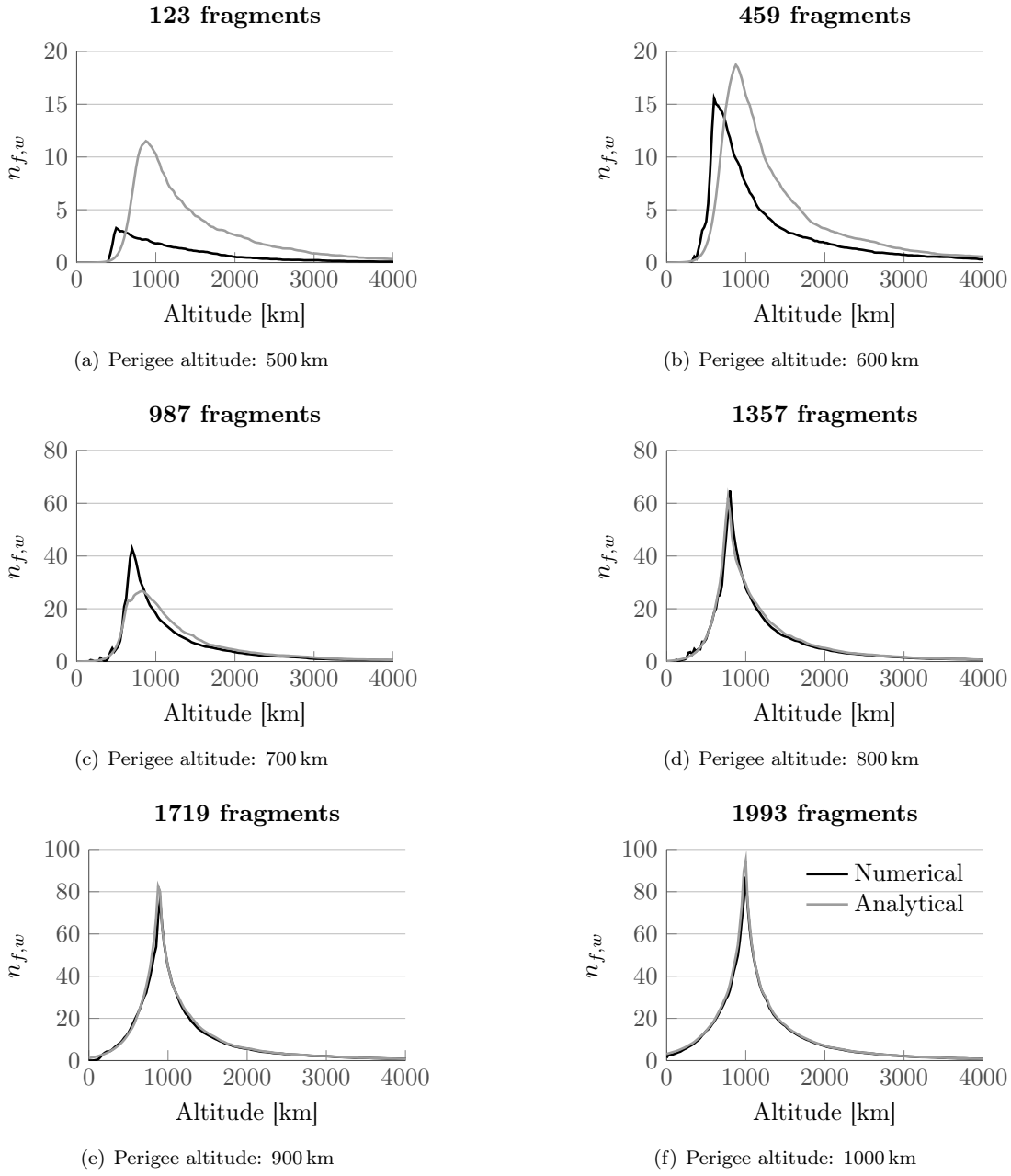

(a) Perigee altitude: 500 km

(b) Perigee altitude: 600 km

(c) Perigee altitude: 700 km

(d) Perigee altitude: 800 km

(e) Perigee altitude: 900 km

(f) Perigee altitude: 1000 km

Fig. 17 Cloud density expressed in fragment number after 1000 days from the band formation for six different collision altitudes.

smaller than 20% for less than 10 days; for the cases up to 700 km the maximum simulation length is always lower than 6 months, while for the cases at 850 km and higher altitudes the method is able to model the cloud evolution for more than 10 years.

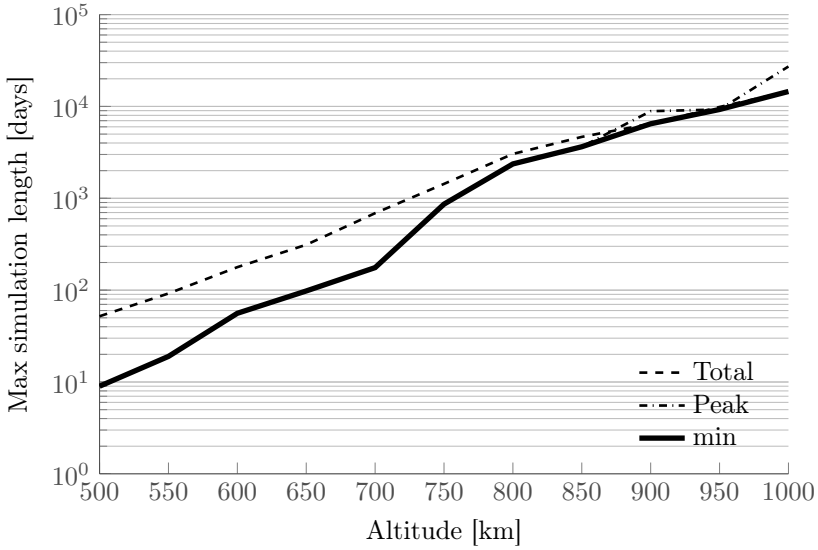

Fig. 18 Maximum simulation length, as a function of the fragmentation altitude.

VI. Discussion on the effect of eccentricity

This section discusses the impact on the method accuracy of the assumptions made to obtain the analytical solution in Equation 27. Two hypotheses were introduced: the fragments are on circular orbits (Equation 22) and the distance of the fragments can be approximated with a fixed distance in part of the expression for the radial velocity to obtain the characteristic of the system (Equation 25). The contribution of each hypothesis is studied in Figure 19, where the variation in the semi-major axis after one period due to drag is plotted as a function of the semi-major axis. The plot is obtained considering that, starting from the altitude where the fragmentation occurs (in this case 500 km), it is possible to compute the maximum eccentricity that a fragment can have, given the semi-major axis of its orbit. In fact, all the fragments' orbits must include the point of fragmentation, which, in the two extreme cases, can be the apogee (Figure 19a) or the perigee (Figure 19b) of the fragment orbit. The maximum eccentricity is then the one associated with one of these two extreme cases: the fragmentation altitude is at the apogee for fragments with semi-major axis lower than the one of the parent orbit, whereas the fragmentation altitude is at the perigee for fragments with semi-major axis higher than the initial one. Knowing both the initial semi-major axis and the eccentricity, the decay of the fragment in one period can be computed; the value of the area-to-mass ratio is set equal to $0.5\,\mathrm{m^2\,kg^{-1}}$.

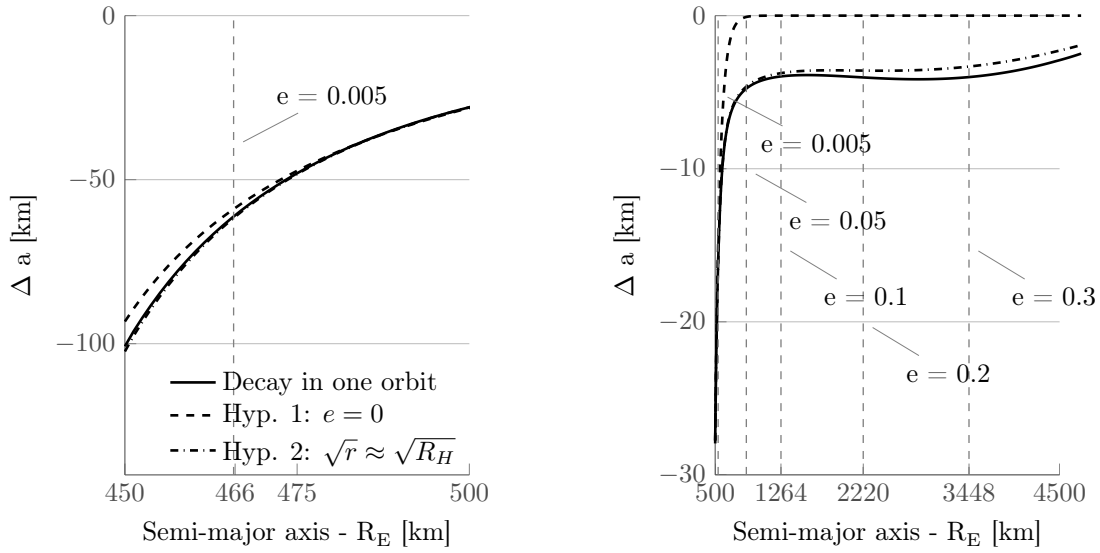

Fig. 19 Variation of the semi-major axis in one orbit as a function of the orbit semi-major axis with different hypotheses for the integration, considering a fragmentation at 500 km. (a) refers to semi-major axis values lower than the fragmentation altitude, (b) to higher semi-major axis values. The vertical lines refer to eccentricity values.

In Figure 19 the vertical lines indicate the eccentricity. The solid curve indicates the variation of the semi-major axis a obtained through numerical integration of Gauss' equations for a and the eccentricity e.

The dashed curve is obtained through numerical integration of Gauss' equations for a and the eccentricity e, but assuming $\sqrt{r} \approx \sqrt{R_H}$: as shown in Figure 19, this hypothesis introduces a small but acceptable error.

The dash-dotted curve represents the effect of the hypothesis $e = 0$ that is the integration only of

$$v_r = -\varepsilon\sqrt{a}\exp\Big(-\frac{a}{H}\Big) \tag{36}$$

and it is possible to observe that the fragment decay is underestimated, both at high and at low altitude. This is due to the fact that neglecting the eccentricity in the exponential term corresponds to applying an incorrect value of the density to compute the drag effect, as shown in Figure 19(b). In fact, using only the value of the semi-major axis, the information on the passage with low perigee, given by the eccentricity, is lost and the predicted decay is null.

For example, for a fragment with semi-major axis equal to $R_E + 1000\,\text{km}$ and corresponding eccentricity equal to 0.007, Gauss's equations estimate a reduction of the semi-major axis of 4.40 km in 94 minutes. Introducing the approximation $\sqrt{r} \approx \sqrt{R_H}$, the predicted decay is 4.24 km, so the relative error is less than 4%. On the other end, with the hypothesis of circular orbit, the predicted decay is almost zero (0.11 km) and so the effect of drag on the cloud is largely underestimated.

This effect is stronger at low altitude where a small variation in altitude results in a larger variation in density compared to what happens at higher altitude; in other words, at low altitudes the eccentricity value above which the decay is strongly underestimated is lower than at high altitude.

One could expect drag to affect the eccentricity distribution in such a way that the average eccentricity is reduced with time because of the progressive circularization of the orbits. Actually, as shown in Figure 20, drag reduces the number of fragments, but especially those with low eccentricity as they also have low semi-major axis. The fragments with high eccentricity instead also have high energy and their decay is slow; their presence drives the average eccentricity to increase (for example, in the case in Figure 20 from 0.05 to 0.08). This means that the error due to eccentricity always increases with the simulation time.

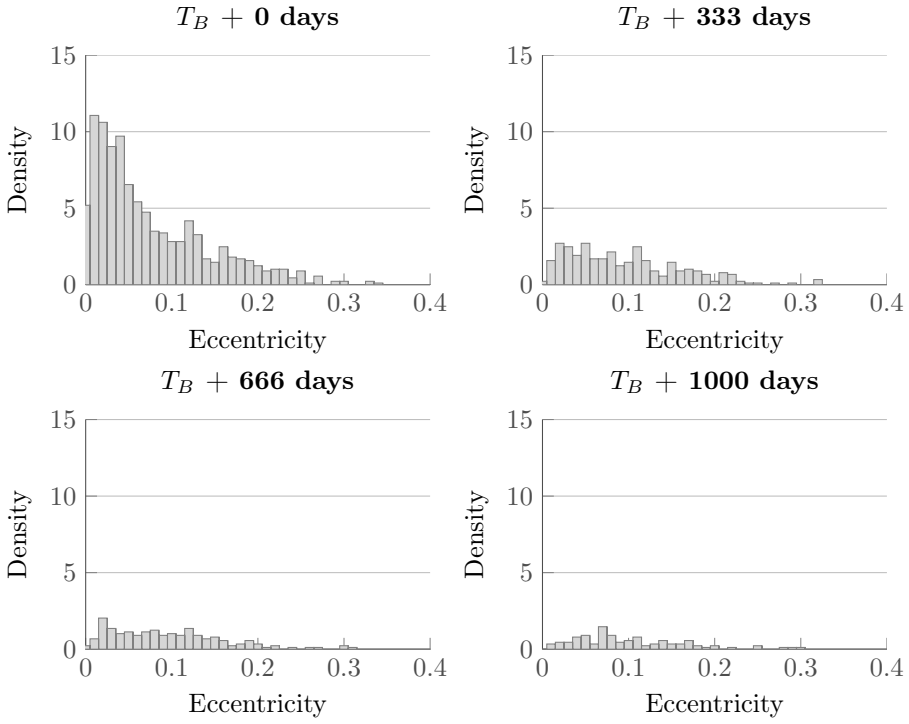

Fig. 20 Evolution of the eccentricity distribution as a function of time, after the band formation, for a fragmentation at 500 km**.**

Current work is aiming at including the eccentricity into the continuity equation, so that the method could be improved also at low altitudes. In this case, a full analytical formulation is not possible, in particular to express the characteristics of the new system. However, they can be expressed with known numerical functions that can be easily implemented and have a limited impact on the computational time.

VII. Conclusions

Obtaining a reliable picture of the future debris environment requires the inclusion of small fragments ($< 10\,\text{cm}$) in long-term projections. Given the large number of fragments, simplified models have been studied to reduce the computational time required by simulations. In this work, an analytical method is proposed to obtain the evolution of a debris cloud generated by a collision.

The starting point for the method is the NASA breakup model, which provides the features of the fragments generated by a non-catastrophic collision; only the fragments whose size is between 1 mm and 8 cm were considered. The fragment orbital parameters were numerically propagated, accounting for the effect of atmospheric drag and the Earth's oblateness, until the distribution of the fragments could be considered spherically symmetrical and drag was the most relevant perturbation for fragment evolution. The information on fragment position is translated into a continuous function, using an analytical expression for the fragment density probability along the orbit. Starting from the initial condition at the band formation, the evolution of the cloud density with time, under the effect of atmospheric drag, is obtained through the continuity equation. Under the hypothesis of circular orbits and considering an exponential model for the atmosphere, it is possible to derive an analytical expression for the fragment density as a function of time.

The method was validated through a comparison with the numerical propagation. For fragmentations occurring at altitudes higher than 800 km, the analytical method shows good accuracy for simulations up to 1000 days after the band formation, keeping the simulation time lower than 10% of the computational time of the numerical propagation. At lower altitudes, the hypothesis of circular orbits introduces a larger error that suggests that eccentricity should be included in the analytical propagation. Future work will further develop the proposed method, for example trying to include

also the effect of solar radiation pressure, which is relevant for the debris motion at altitudes above 800 km.

The present results suggest that the method may become an efficient tool to simulate a large array of collision scenarios. Indeed, many simulations can be performed varying the fragmentation conditions (e.g., altitude, inclination and impact energy). This can help to better understand the fragments' dynamics, to assess under which conditions a fragmentation event is more dangerous to operational satellites and to identify orbiting objects that, in case of fragmentation, are more likely to generate a debris cloud that can intersect other spacecraft and pose a hazard.

VIII. Acknowledgement

Francesca Letizia is supported by the Amelia Earhart Fellowship for the academic year 2013/2014. C. Colombo acknowledges the support received by the Marie Curie grant 302270 (SpaceDebECM - Space Debris Evolution, Collision risk, and Mitigation) within the 7^{th} European Community Framework Programme.

IX. References

[1] Krisko, P. H., "The predicted growth of the low-Earth orbit space debris environment – an assessment of future risk for spacecraft," *Proceedings of the Institution of Mechanical Engineers, Part G: Journal of Aerospace Engineering*, Vol. 221, No. 6, Jan. 2007, pp. 975–985, doi:10.1243/09544100JAERO192.

[2] Pardini, C. and Anselmo, L., "Review of past on-orbit collisions among cataloged objects and examination of the catastrophic fragmentation concept," *International Astronautical Congress*, Beijing, Sept. 2013, IAC-13.A6.2.9.

[3] NASA Orbital Debris Program Office, "A New Collision in Space?" *Orbital Debris Quaterly News*, Vol. 7, No. 3, 2002, pp. 1–2, http://orbitaldebris.jsc.nasa.gov/newsletter/pdfs/ODQNv7i3.pdf [retrieved 01 April 2014].

[4] NASA Orbital Debris Program Office, "Two Derelict NOAA Satellites Experience Anomalous Events," *Orbital Debris Quaterly News*, Vol. 16, No. 1, 2012, pp. 1–2, http://orbitaldebris.jsc.nasa.gov/newsletter/pdfs/ODQNv16i1.pdf [retrieved 01 April 2014].

[5] NASA Orbital Debris Program Office, "Small Satellite Possibly Hit by Even Smaller Object," *Orbital Debris Quaterly News*, Vol. 17, No. 2, 2013, pp. 1, http://orbitaldebris.jsc.nasa.gov/newsletter/pdfs/ODQNv17i2.pdf [retrieved 01 April 2014].

[6] Martin, C., Walker, R., and Klinkrad, H., "The sensitivity of the ESA DELTA model," *Advances in Space Research*, Vol. 34, No. 5, Jan. 2004, pp. 969–974, doi:10.1016/j.asr.2003.02.028.

[7] White, A. E. and Lewis, H. G., "The many futures of active debris removal," *Acta Astronautica*, Vol. 95, Feb. 2014, pp. 189–197, doi:10.1016/j.actaastro.2013.11.009.

[8] Rossi, A., Cordelli, A., and Pardini, C., "Modelling the space debris evolution: Two new computer codes," *Advances in the Astronautical Sciences - Space Flight Mechanics*, Albuquerque, April 1995.

[9] Lewis, H., Swinerd, G., Williams, N., and Gittins, G., "DAMAGE: a dedicated GEO debris model framework," *Third European Conference on Space Debris*, Darmstadt, March 2001, pp. 373–378.

[10] King-Hele, D., "Orbital theory for a spherically symmetrical exponential atmosphere," *Satellite orbits in an atmosphere: theory and application*, Blackie, Glasgow and London, 1987, pp. 44–62.

[11] Cordelli, A., Farinella, P., and Rossi, A., "Study on Long Term Evolution of Earth Orbiting Debris," Study note of work package 3200, ESA/ESOC Contract No. 10034/92/D/IM(SC), 1995.

[12] Kebschull, C., Braun, V., Flegel, S. K., Gelhaus, J., Möckel, M., Radtke, J., Wiedemann, C., Krag, H., Carnelli, I., and Voersmann, P., "A Simplified Approach to Analyze the Space Debris Evolution in the Low Earth Orbit," *International Astronautical Congress*, Beijing, Sept. 2013, IAC-13.A6.2.3.

[13] Rossi, A., Valsecchi, G. B., Anselmo, L., Pardini, C., Lewis, H. G., and Colombo, C., "Fragmentation Consequence Analysis for LEO and GEO Orbits," *GreenOps Workshop*, Noordwijk, Nov. 2013, ESA AO 1/7121/12/F/MOS.

[14] Hoots, F. R. and Hansen, B. W., "Satellite breakup debris cloud characterization," *24th AAS/AIAA Space Flight Mechanics Meeting*, Santa Fe, Jan. 2014, AAS 14-329.

[15] Valk, S., Lemaître, A., and Deleflie, F., "Semi-analytical theory of mean orbital motion for geosynchronous space debris under gravitational influence," *Advances in Space Research*, Vol. 43, No. 7, April 2009, pp. 1070–1082, doi:10.1016/j.asr.2008.12.015.

[16] Izzo, D., *Statistical modelling of orbits and its application to trackable objects and to debris clouds*, Ph.D. thesis, Università La Sapienza, 2002.

[17] Liou, J.-C., "An active debris removal parametric study for LEO environment remediation," *Advances*

in Space Research, Vol. 47, No. 11, 2011, pp. 1865 – 1876,
doi:10.1016/j.asr.2011.02.003.

[18] Foster, J. L., "The analytic basis for debris avoidance operations for the International Space Station," *Third European Conference on Space Debris*, Darmstadt, 2001, pp. 441–445.

[19] Chobotov, V., "Space debris," *Orbital mechanics*, AIAA, Reston, 3rd ed., 2002, pp. 301–334, ISBN: 1563475375.

[20] McInnes, C. R., "An analytical model for the catastrophic production of orbital debris," *ESA Journal*, Vol. 17, No. 4, 1993, pp. 293–305.

[21] Gor'kavyi, N., "A new approach to dynamical evolution of interplanetary dust," *The Astrophysical Journal*, Vol. 474, No. 1, 1997, pp. 496–502,
doi:10.1086/303440.

[22] Gor'kavyi, N., Ozernoy, L., Mather, J., and Taidakova, T., "Quasi-stationary states of dust flows under Poynting-Robertson drag: New analytical and numerical solutions," *The Astrophysical Journal*, Vol. 488, No. 1, 1997, pp. 268–276.

[23] McInnes, C. R., "Simple analytic model of the long term evolution of nanosatellite constellations," *Journal of Guidance Control and Dynamics*, Vol. 23, No. 2, 2000, pp. 332–338.

[24] Colombo, C. and McInnes, C. R., "Evolution of swarms of smart dust spacecraft," *New Trends in Astrodynamics and Applications VI*, Courant Institute of Mathematical Sciences, New York, June 2011.

[25] Johnson, N. L. and Krisko, P. H., "NASA's new breakup model of EVOLVE 4.0," *Advances in Space Research*, Vol. 28, No. 9, 2001, pp. 1377–1384,
doi:10.1016/S0273-1177(01)00423-9.

[26] Krisko, P. H., "Proper Implementation of the 1998 NASA Breakup Model," *Orbital Debris Quarterly News*, Vol. 15, No. 4, 2011, pp. 1–10.

[27] Rossi, A., "NASA Breakup Model Implementation: Comparison of results," *24^{t}h Inter-Agency Space Debris Coordination Committee Meeting*, Tsukuba, April 2006.

[28] Schäfer, F., Quarti, M., Roll, M., Matura, P., Rudolph, M., Putzar, R., Reichel, M., Hupfer, J., and Buehler, K., "Fragmentation studies of simple cubic structures at Fraunhofer EMI," *Sixth European Conference on Space Debris*, Darmstadt, April 2013.

[29] Liou, J. C., Fitz-Coy, N., Clark, S., Werremeyer, M., Huynh, T., Sorge, M., Voelker, M., and Opiela, J., "DebriSat - A planned laboratory based satellite impact experiment for breakup fragment characterization," *Sixth European Conference on Space Debris*, Darmstadt, April 2013.

[30] Sdunnus, H., Beltrami, P., Klinkrad, H., Matney, M., Nazarenko, A., and Wegener, P., "Comparison of debris flux models," *Advances in Space Research*, Vol. 34, No. 5, Jan. 2004, pp. 1000–1005, doi:10.1016/j.asr.2003.11.010.

[31] Sorge, M. E., "Satellite Fragmentation Modeling with IMPACT," *AIAA/AAS Astrodynamics Specialist Conference*, Honolulu, Aug. 2008.

[32] Jehn, R., "Dispersion of debris clouds from In-orbit fragmentation events," *ESA Journal*, Vol. 15, No. 1, 1991, pp. 63–77.

[33] Vallado, D. A., *Fundamentals of astrodynamics and applications*, Springer, 4th ed., 2013, ISBN: 978-1881883180.

[34] Gentle, J. E., "Estimation of functions," *Elements of computational statistics*, Springer, 2002, pp. 146–161, ISBN: 0-387-95489-9.

[35] Chobotov, V., "Dynamics of orbiting debris clouds and the resulting collision hazard to spacecraft," *Journal of the British Interplanetary Society*, Vol. 43, 1990, pp. 187–195.

[36] McKnight, D. S., "A phased approach to collision hazard analysis," *Advances in Space Research*, Vol. 10, No. 3-4, Jan. 1990, pp. 385–388, doi:10.1016/0273-1177(90)90374-9.

[37] Ashenberg, J., "Formulas for the phase characteristics in the problem of low-Earth-orbital debris," *Journal of Spacecraft and Rockets*, Vol. 31, No. 6, Nov. 1994, pp. 1044–1049, doi:10.2514/3.26556.

[38] Letizia, F., Colombo, C., Lewis, H. G., and McInnes, C. R., "Debris cloud evolution in Low Earth Orbit," *International Astronautical Congress*, Beijing, Sept. 2013, IAC-13.A6.P.12.

[39] McInnes, C. R. and Colombo, C., "Wave-like patterns in an elliptical satellite ring," *Journal of Guidance, Control, and Dynamics*, Vol. 36, No. 6, 2013, pp. 1767–1771, doi:10.2514/1.55956.